


 Cite this: *Lab Chip*, 2015, 15, 3776

## A digital microfluidic device with integrated nanostructured microelectrodes for electrochemical immunoassays†

 Darius G. Rackus,<sup>ab</sup> Michael D. M. Dryden,<sup>a</sup> Julian Lamanna,<sup>a</sup> Alexandre Zaragoza,<sup>c</sup> Brian Lam,<sup>c</sup> Shana O. Kelley<sup>\*acde</sup> and Aaron R. Wheeler<sup>\*abd</sup>

Nanostructured microelectrodes (NMEs) are three-dimensional electrodes that have superb sensitivity for electroanalysis. Here we report the integration of NMEs with the versatile fluid-handling system digital microfluidics (DMF), for eventual application to distributed diagnostics outside of the laboratory. In the new methods reported here, indium tin oxide DMF top plates were modified to include Au NMEs as well as counter and pseudoreference electrodes. The new system was observed to outperform planar sensing electrodes of the type that are typically integrated with DMF. A rubella virus (RV) IgG immunoassay was developed to evaluate the diagnostic potential for the new system, relying on magnetic microparticles coated with RV particles and analysis by differential pulse voltammetry. The limit of detection of the assay ( $0.07 \text{ IU mL}^{-1}$ ) was  $>100\times$  below the World Health Organization defined cut-off for rubella immunity. The sensitivity of the integrated device and its small size suggest future utility for distributed diagnostics.

 Received 14th June 2015,  
Accepted 24th July 2015

DOI: 10.1039/c5lc00660k

[www.rsc.org/loc](http://www.rsc.org/loc)

### Introduction

Miniaturized analytical devices providing rapid sample-to-answer processing are necessary for the emerging paradigm of distributed (as opposed to centralized) diagnosis.<sup>1,2</sup> Electrochemical detectors, which are small, portable, and inexpensive, are the detection modality of choice for these kinds of devices.<sup>3</sup> The blood glucose meter is perhaps the most widely used and successful example of such a sample-to-answer electrochemical device.<sup>4,5</sup> It has revolutionized the lives and care of diabetics and has an estimated global market value of \$11 billion.<sup>6</sup> While the glucose meter is an unmitigated success, the distributed diagnosis revolution has not yet gone mainstream for the detection of proteins and nucleic acids, which can be important biomarkers for disease states. Although label-free approaches have been developed for

proteins and nucleic acids,<sup>7–9</sup> electrochemical detection of these analytes is primarily by affinity assays that rely on the capture of the target analyte, requiring multiple wash steps and labelling reagents. Additionally, concentrations of these analytes are much lower compared to blood glucose. Novel electrochemical approaches and developments in microfluidics are being used to meet these challenges.<sup>6,10</sup>

Many new electrochemical approaches are centred on advances in electrode materials. One example is the nanostructured microelectrode (NME), which has been used for the sensitive detection of nucleic acids, proteins, and small molecules.<sup>11</sup> NMEs are formed from the electrodeposition of metal through constricted apertures on the micrometer length-scale.<sup>12</sup> Their three-dimensional microstructure penetrates into the solution and can be nanotextured, resulting in increased surface area. This increases electron transfer rates and creates more sites for the deposition of molecular probes. NMEs have been used for the rapid detection of aM concentrations of nucleic acids<sup>13,14</sup> and pM concentrations of proteins.<sup>15</sup> Because of their high sensitivity, NMEs are ideal for applications such as distributed diagnostics and personalized medicine in which small sample volumes are desirable. As such, their utility would be greatly augmented by coupling with a versatile small-volume fluid handling system such as digital microfluidics (DMF).

DMF is a liquid handling technology used to manipulate discrete droplets of nL– $\mu\text{L}$  volume. In the (most common) two-plate format, droplets are sandwiched between hydrophobic top and bottom plates. The bottom plate typically

<sup>a</sup> Department of Chemistry, University of Toronto, 80 St. George St., Toronto, ON, M5S 3H6, Canada. E-mail: shana.kelley@utoronto.ca, aaron.wheeler@utoronto.ca; Tel: +1 (416) 978 8641 (S.O.K.), +1 (416) 946 3864 (A.R.W.)

<sup>b</sup> Donnelly Centre for Cellular and Biomolecular Research, University of Toronto, 160 College St., Toronto, ON, M5S 3E1, Canada

<sup>c</sup> Department of Pharmaceutical Sciences, Leslie Dan Faculty of Pharmacy, University of Toronto, 144 College St., Toronto, ON, M5S 3M2, Canada

<sup>d</sup> Institute for Biomaterials and Biomedical Engineering, University of Toronto, 164 College St., Toronto, ON, M5S 3G9, Canada

<sup>e</sup> Department of Biochemistry, Faculty of Medicine, University of Toronto, 1 King's College Circle, Toronto, ON, M5S 1A8, Canada

† Electronic supplementary information (ESI) available. See DOI: 10.1039/c5lc00660k

contains DMF driving electrodes (that determine the size and shape of the droplets) covered by a dielectric insulator, and the top plate, generally formed from transparent indium–tin–oxide (ITO) coated glass, serves as a DMF counter-electrode. Droplets are moved by electrostatic forces generated by the application of electrical potentials between DMF driving electrodes and the DMF counter electrode.<sup>16</sup> DMF devices have a generic architecture that (with little modification) can be used for applications ranging from chemical analysis,<sup>17–21</sup> to cell culture,<sup>22–24</sup> and chemical synthesis.<sup>25–27</sup> DMF is well suited to use with bioanalytical techniques such as immunoassays<sup>28</sup> which involve multiple reagents and repetitive wash steps. Magnetic bead-based immunoassays are particularly well suited to DMF,<sup>29</sup> with numerous examples in the literature utilizing fluorescent,<sup>30,31</sup> chemiluminescent,<sup>32–34</sup> and electrochemical<sup>20</sup> detection modalities. While electrochemistry is particularly attractive for the reasons described above, the one geometry used for this application previously<sup>20</sup> (featuring small, planar electrodes) was found to suffer from high detection limits and poor sensitivity.

Here, we report the first integration of NMEs into a DMF device to combine sensitive electrochemical detection with discrete fluid handling. New methods were required to fabricate NMEs and DMF devices together, and we demonstrate the advantage of using the new hybrid system over comparable microfabricated planar electrodes. We validated the performance of the hybrid devices for a proof-of-principle electrochemical ELISA for rubella virus (RV) diagnosis. We propose that this marriage of DMF for flexible control over complex sample processing regimens and NME electroanalysis for high-sensitivity detection is a useful step toward the goal of distributed diagnostics.

## Experimental

### Materials and reagents

General reagents were from Sigma Aldrich (Oakville, ON). Microposit MF-312 developer and S1811 positive photoresist were from Rohm and Haas (Marlborough, MA), AZ 300T stripper was from AZ Electronic Materials (Somerville, NJ), KI/I<sub>2</sub> Au etchant was from Transene, Inc. (Denver, CO), CR-4 Cr etchant was from Cyantek (Freemont, CA), SU-8 3005 negative photoresist and developer were from MicroChem Corp. (Newton, MA), and positive photoresist PR1-12000A was from Futurrex, Inc. (Franklin NJ). RV coated magnetic beads and anti-RV IgG calibration standards were generously provided by Abbott Laboratories (Abbot Park, IL). Pluronic L-64 (BASF Corp.) was generously donated by Brenntag Canada (Toronto, ON). Deionized water (di-H<sub>2</sub>O) had a resistivity of 18 MΩ cm at 25 °C. All electrochemical measurements were carried out using a PalmSens3 potentiostat (PalmSens BV, Utrecht, NL).

### Device fabrication

DMF devices were fabricated in the Toronto Nanofabrication Centre (TNFC) cleanroom facility at the University of Toronto using transparent photomasks printed at Pacific Arts and

Design (Markham, ON) at a resolution of 20 000 DPI. Devices comprised two parts: a bottom plate containing an array of DMF driving-electrodes for droplet actuation, and a top plate with sensing electrodes (some used for growing NMEs) and a DMF counter-electrode for droplet movement. The bottom plates were fabricated using methods similar to those described previously.<sup>20,34,35</sup> Unlike previous techniques, the hydrophobic layer was prepared by spin-coating Fluoropel 1604V (Cytonix, LLC, Beltsville, MD) (1% w/v in PFC110, 3000 rpm, 30 s) and then baking on a hot plate (130 °C, 10 min). When completed, the design featured an array of 80 Cr actuation electrodes (2.2 × 2.2 mm ea.) connected to 8 reservoir electrodes (16.4 × 6.7 mm ea.) and 4 waste reservoir electrodes (16.4 × 6.4 mm ea.). The actuation electrodes were roughly square with interdigitated borders (180 μm peak to peak sinusoids) and inter-electrode gaps of 30–80 μm.

DMF top plates were formed from 50 × 75 mm ITO coated glass slides ( $R_s = 8\text{--}12 \Omega \text{ m}^{-1}$ ) (Delta Technologies, Ltd., Loveland, CO) that had been modified at Telic Co. (Valencia, CA) such that the ITO was coated with 10 nm of Cr, 100 nm of Au, and a layer of photoresist AZ 1500. The plates were patterned using four photolithography steps, each followed by etching or liftoff. In the first photolithography step (to define the sensing electrodes), the substrates were exposed with UV light for 10 s, then developed for 20 s in a 1:1 mixture of MF-312:H<sub>2</sub>O developer. The Au layer was then etched with KI/I<sub>2</sub> Au etchant, the substrates were rinsed in di-H<sub>2</sub>O and then the Cr layer was etched using CR-4 etchant. The remaining photoresist was stripped using AZ 300T stripper and the substrates were washed in acetone, isopropyl alcohol (IPA), and di-H<sub>2</sub>O before being dried under a N<sub>2</sub> stream and baked at 95 °C on a hotplate for 2 min. When completed, each sensor featured two rectangular Au electrodes [counter electrode (CE) and reference electrode (RE), both 2.03 mm × 0.24 mm], and three triangular working electrodes (WE, equilateral triangle with side length of 0.42 mm). For the second photolithography step (to define the ITO DMF counter-electrode), photoresist S1811 was spin-coated (3000 rpm, 30 s) onto the devices, which were baked on a hot plate at 95 °C for 1 min. The substrates were exposed with broad-band UV light for 10 s, developed as above, and then the ITO was etched at room temperature in a 4:2:1 mixture (by volume) of HCl:H<sub>2</sub>O:HNO<sub>3</sub> for 8 min. The remaining photoresist was stripped in AZ 300T and the substrates were rinsed with acetone, IPA, and di-H<sub>2</sub>O. When completed, the contiguous ITO pattern was in the form of an irregular polygon that covered most of the substrate, but with a border of bare glass (minimum width 250 μm) isolating it from the sensing electrodes. For the third photolithography step (to define apertures above the sensing electrodes), SU-8 3005 was spin-coated at 2000 rpm for 30 s, and the substrates were baked on a hotplate at 95 °C for 2 min. The substrates were then exposed with broad-band UV light through a photomask for 20 s and developed in SU-8 developer for 2 min. When completed, the substrate featured T-shaped islands of SU-8 (4.1 mm × 3.8 mm and 8 μm thick) positioned over each group of sensing

electrodes, and each island included five apertures – two with rectangular shape (1.38 mm × 120 μm) above the CE and RE, and three with circular shape (30 μm in diameter) above the WEs. For the fourth photolithography step (to apply a patterned hydrophobic coating), photoresist PR1-12000A was spin coated (2300 rpm, 40 s) before a softbake on a hot plate at 120 °C for 3 min. The substrates were exposed by UV light through a photomask for 65.6 s and then developed in a 1:1 mixture of MF-312 and H<sub>2</sub>O. After rinsing with di-H<sub>2</sub>O and drying under N<sub>2</sub> stream, Fluoropel 1604V was spincoated (1% w/v in PFC110, 2000 rpm, 40 s). Substrates were baked on a hot plate at 125 °C for 10 min, allowed to cool, and then lift-off was performed by removing the underlying photoresist in a stream of acetone. The finished top plates were rinsed with di-H<sub>2</sub>O, dried under N<sub>2</sub> stream, and allowed to bake on a hot plate at 125 °C for a further 10 min. When completed, the entire substrate was coated with FluoroPel, except for a rectangular area (1.5 mm × 2.1 mm) over each set of sensing electrodes.

### NME preparation and characterization

NMEs were formed by electrodeposition onto triangular WEs on DMF top plates (described above) at room temperature using a three-electrode system comprising an external Ag/AgCl reference electrode and a Pt wire counter electrode. A 50 μL droplet of plating solution (20 mM HAuCl<sub>4(aq)</sub> in 0.5 M HCl<sub>(aq)</sub>) was positioned on the surface. NMEs were plated onto the triangular WE traces at 0.0 V vs. Ag/AgCl until the current was measured to be -5.5 μA. NMEs were imaged at the Centre for Nanostructure Imaging at the University of Toronto using a Hitachi TM-1000 table top variable pressure scanning electron microscope (Hitachi, Mississauga) operating at 15 kV.

### Electrode comparisons

Glass substrates bearing planar working electrodes were fabricated in two photolithography/etching steps in the TNFC cleanroom on 50 × 75 mm glass slides coated with layers of Cr (10 nm), Au (100 nm), and photoresist AZ 1500 (Telic Co.). For the first photolithography step (to define the electrode patterns), each substrate was exposed to UV light for 10 s using a mask aligner before developing in a 1:1 mixture of MF-312 and di-H<sub>2</sub>O for 20 s. The Au was etched with KI/I<sub>2</sub> etchant. The substrate was rinsed in di-H<sub>2</sub>O and then the Cr was etched using CR-4 etchant. Remaining photoresist was stripped using AZ 300T stripper. The substrates were washed in acetone, IPA, and di-H<sub>2</sub>O before drying under N<sub>2</sub> stream and baked at 95 °C on a hotplate for 2 min. When completed, each electrode measured 2 mm in diameter. For the second photolithography step (to define apertures above the electrodes), SU-8 3005 was spin-coated at 2000 rpm for 30 s, and the substrates were baked at 95 °C on a hotplate for 2 min. The substrates were then exposed with UV light through a photomask for 20 s and developed in SU-8 developer for 2 min. The substrate was then washed in acetone, IPA, and di-

H<sub>2</sub>O before drying under a N<sub>2</sub> stream. When completed, the substrate was covered with SU-8 with circular apertures (798 μm dia.) above the working electrodes and rectangular apertures (2 × 75 mm) at the edge of the device for electrical connections.

The performance of planar electrodes was compared with NMEs by cyclic voltammetry (CV) using a three-electrode setup with an external Ag/AgCl reference electrode and a Pt wire counter electrode. Non-DMF planar electrodes (described above), DMF top plates without NMEs (known as “footprints”), and DMF top-plates with NMEs were used as working electrodes. CV was carried out using a 2.5 mM solution of K<sub>3</sub>Fe(CN)<sub>6(aq)</sub>, scanning from -0.1 to +0.7 V (vs. Ag/AgCl) at a scan rate of 100 mV s<sup>-1</sup>.

### Device assembly and operation

Each NME-DMF device was assembled as shown in Fig. 1 from a DMF bottom plate and an NME-bearing top plate separated by spacers created from two pieces of 3 M Scotch double-sided tape (St. Paul, MN) with a total spacer thickness of 180 μm. In this orientation, unit droplets (*i.e.*, droplets that cover a single DMF driving electrode) had volumes of ~900 nL. For droplet movement and control, the device was interfaced by pogo pins to an automation system (described in detail elsewhere<sup>34,35</sup>). Droplets were actuated by applying a preprogrammed sequence of voltages (85–110 V<sub>RMS</sub> 10 kHz sine wave) between the top plate DMF counter-electrode and the bottom plate DMF driving electrodes. A magnet on a motorized stage beneath the device was used for particle separations as described previously.<sup>34,35</sup> Each step of the immunoassay was carried out by calling preprogrammed sequences of droplet movement and particle separations.

### Immunoassays

All solutions used in immunoassays (described below) were modified to contain 0.05% (w/v) Pluronic L64. Virus-coated paramagnetic particles and RV IgG calibrators were adapted from the Architect rubella virus IgG assay kit from Abbot Laboratories. Reagents from other vendors included Superblock Tris-buffered saline (TBS), anti-human alkaline phosphatase conjugated IgG, 4-aminophenyl phosphate monohydrate (Santa Cruz Biotechnology, Inc., Dallas, TX). Prior to conducting immunoassays, RV coated paramagnetic particles were concentrated to ~3.0 × 10<sup>8</sup> particles mL<sup>-1</sup> and washed twice with Superblock TBS containing 0.05% (w/v) Pluronic L64 as described previously.<sup>33–35</sup> Stock RV IgG calibrators were used to prepare solutions of 0, 5, 7.5, 10, 15, 125, and 250 IU mL<sup>-1</sup> standards. Samples were prepared by diluting these standards ten-fold in Superblock TBS. A DMF-compatible wash buffer was prepared comprising 25 mM Tris-HCl and 130 mM NaCl, pH 7.4. Conjugate diluent was prepared as previously described.<sup>33,34</sup> Working solutions of conjugate were prepared by diluting alkaline phosphatase-conjugated goat anti-human IgG 1:5000 with the conjugate diluent. The substrate solution, comprising 0.5 mM

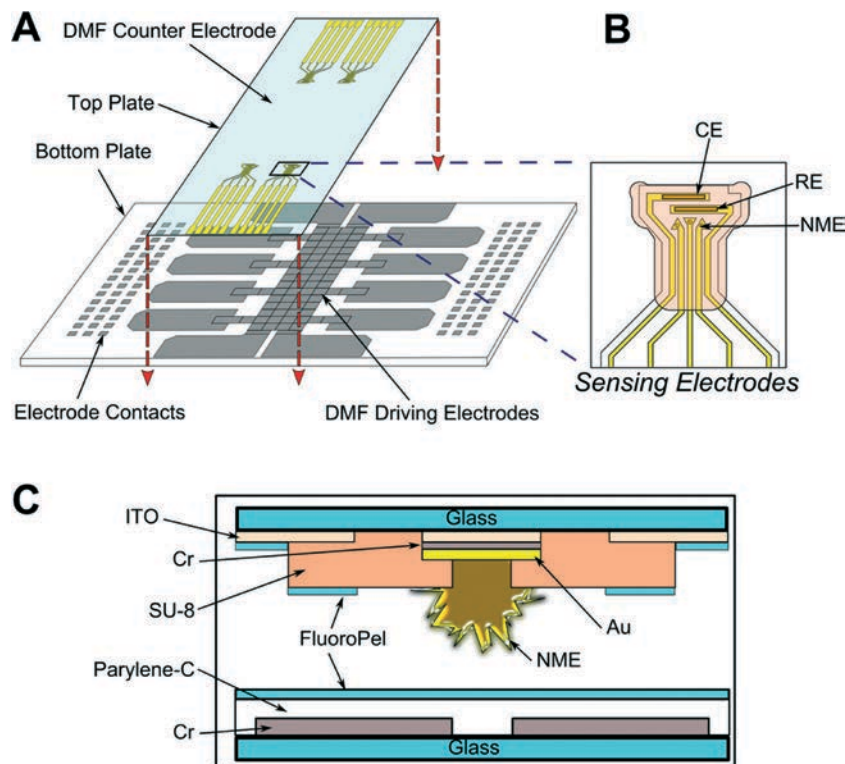


**Fig. 1** Overview of DMF device with integrated nanostructured microelectrodes (NMEs). (A) Computer rendering of the device showing the position of four sets of sensing electrodes on the top plate with respect to the DMF bottom plate (red dashed arrows indicate how the two plates are mated). Electrode contacts are used for integration with the automation control system. (B) Cartoon schematic of one set of sensing electrodes, comprising three NMEs, a reference (RE) and a counter electrode (CE). A layer of SU-8 insulates the Au tracings and defines the apertures for NME growth as well as the areas of the CE and RE. The sensing electrodes are surrounded by the ITO DMF counter-electrode. (C) Cartoon (not to scale) schematic of a cross-section of the device showing the layers of the device. On the bottom plate, Cr DMF driving electrodes are covered by an insulating layer of Parylene-C and hydrophobic FluoroPel. The top plate comprises three conducting layers (ITO, Cr, and Au), an insulating layer of SU-8 and a patterned layer of FluoroPel.

*p*-aminophenyl phosphate, 50 mM Tris-HCl, 10 mM NaCl, and 10 mM MgCl<sub>2</sub>, pH 9.0, was prepared, aliquoted, and stored at -20 °C until needed.

An eight-step procedure was developed to detect RV IgG. (1) A droplet of paramagnetic particles (1.8 μL, formed by dispensing two unit droplets and merging them) was dispensed from a reservoir, the particles were immobilized, and the supernatant was removed. (2) A droplet of sample (1.8 μL) was dispensed and mixed with the paramagnetic particles for 3 min and separated. (3) Particles were washed four times dispensing 1.8 μL droplets of wash buffer, mixing with the paramagnetic particles, and then immobilizing the particles and removing the supernatant. (4) A droplet of conjugate solution (1.8 μL) was dispensed and mixed with the paramagnetic particles for 2 min and separated. (5) The wash procedure (6) was repeated. (7) A droplet of substrate solution (1.8 μL) was dispensed and mixed with the paramagnetic particles for 20 min and separated for analysis. (8) The supernatant droplet was separated from the particles, moved to one of the sets of sensor electrodes for analysis on-chip by differential pulse voltammetry (DPV). DPV measurements were performed from a range of -200 mV to 350 mV with a potential step of 5 mV, pulse amplitude of 5 mV, and a pulse

period of 5 ms. Peak currents were measured after a linear baseline subtraction between -5 mV and 350 mV. (If no discernible peak was present, the current at 50 mV was used.) Three replicates were measured for each concentration evaluated. Data was analyzed in GraphPad Prism (La Jolla, CA, USA). A four parameter logistic equation was used to fit the data, and the limit of detection (LOD) was calculated as the concentration corresponding to signal  $y_{LOD} = 3\sigma_{blank} + blank$  where  $\sigma_{blank}$  is the standard deviation of the blank, and *blank* is the mean signal of the blank. Limit of quantitation (LOQ) was calculated as the concentration corresponding to signal  $y_{LOD} = 10\sigma_{blank} + blank$ .

## Results and discussion

### DMF-NME device characterization

The goal of this work was to integrate NMEs with a DMF liquid-handling platform for eventual application to distributed diagnostics. Both technologies have their own (sometimes incompatible) requirements. NMEs are formed from electroplating metal through constricted apertures, which requires that the sensing electrodes be coated with a patterned insulating layer. Each electrode must ultimately be

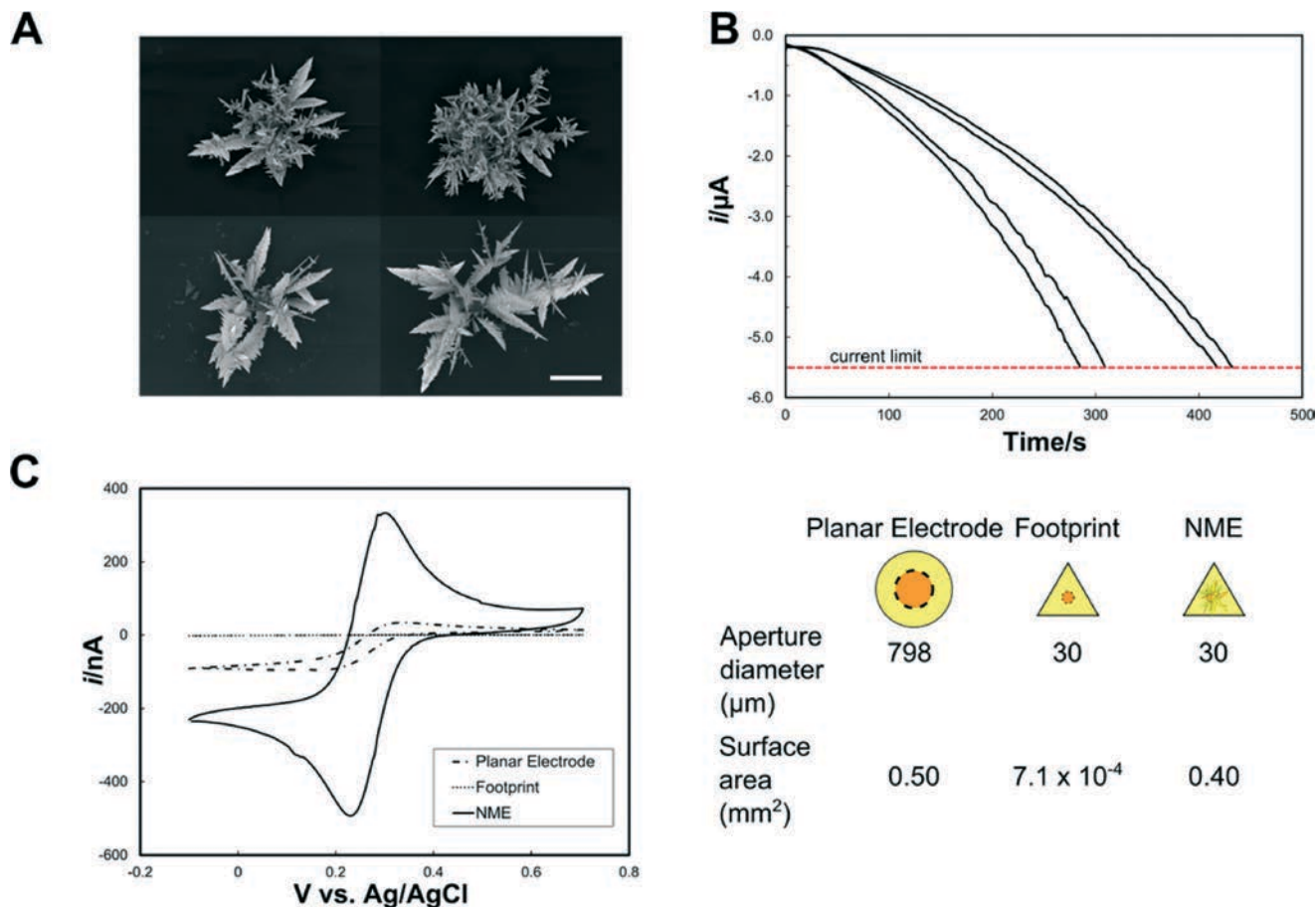


Fig. 2 Characterization of NMEs formed on DMF top plates. (A) Representative scanning electron micrographs of four NMEs plated on DMF top plates. Scale bar = 50  $\mu\text{m}$ . (B) Representative current vs. time plots collected during the electroplating of four NMEs (20 mM  $\text{HAuCl}_4$ , 0.5 M HCl, 0 V vs. Ag/AgCl). In each case, electroplating was continued until a current limit of  $-5.5 \mu\text{A}$  was measured. (C) Representative cyclic voltammograms ( $-0.1 \text{ V}$  to  $+0.7 \text{ V}$   $v = 100 \text{ mV s}^{-1}$ ) (left) generated for 2.5 mM  $\text{K}_3\text{Fe}(\text{CN})_6(\text{aq})$  in  $\text{KNO}_3(\text{aq})$  with a 798  $\mu\text{m}$  diameter planar electrode (hashed) on a DMF top plate, an NME “footprint” (a 30  $\mu\text{m}$  diameter planar electrode, dotted) on a DMF top plate, and an NME electroplated through a 30  $\mu\text{m}$  diameter aperture (solid) on a top plate. Cartoons (right) illustrating the dimensions of the three systems.

able to contact the solution to be measured. In contrast, DMF devices require that an array of driving electrodes be covered with an insulating dielectric layer and a hydrophobic surface – these electrodes should not contact the solution being actuated. There are examples in the literature of DMF devices with electroanalysis electrodes integrated within the same plane as the DMF driving electrodes<sup>18,36</sup> (typically located on the bottom plate), and in initial work, we tried applying similar methods for forming DMF-NME devices, but each of these designs was found to suffer either from poor droplet movement fidelity or clogged apertures preventing NME plating. Thus, in the work reported here, we chose an alternate format in which the sensing electrodes are integrated on the plane of the DMF counter-electrode<sup>20,37</sup> (typically located on the top plate). This allowed the use of unaltered DMF bottom plates (enabling facile droplet movement), while preserving the strict conditions required to form NMEs for the top plate (which is less critical for reproducible droplet movement).

The optimized DMF-NME device design is depicted in Fig. 1A. As shown, the glass bottom plate comprises an array

of Cr electrodes that are patterned by photolithography and coated with an insulating dielectric layer and a thin hydrophobic layer of FluoroPel. The glass top plate consists of a patterned ITO DMF CE and four sets of gold sensing electrodes (each set includes three triangular WEs, one rectangular CE, and one rectangular RE), as shown in Fig. 1B. A small area around the sensing electrodes is covered with an insulator layer of SU-8; this layer is punctuated with circular apertures for forming NMEs. To be amenable to droplet movement, a thin hydrophobic layer of FluoroPel is added to the top plate, and a liftoff procedure is used to remove the FluoroPel covering the sensing electrodes. A cross-section of the completed device with all of its layers is shown in Fig. 1C.

#### NME characterization and performance

NMEs are traditionally prepared by electroplating Au (or other metals) through a small aperture (often  $\sim 5 \mu\text{m}$  in diameter) in a thin insulating layer (often  $\sim 2 \mu\text{m}$  thick), which allows for the generation of electrodes with characteristic

fractal-like geometries with high surface area.<sup>11–15</sup> Unfortunately, in the work described here, the fluorocarbon liftoff technique used to make the top plate hydrophobic (required for DMF) was found to be compatible only with apertures of 30  $\mu\text{m}$  dia. or larger (the fluorocarbon coating could not be cleared from smaller apertures). In initial trials with a thin insulating layer (2  $\mu\text{m}$  SU-8) patterned on DMF top plates punctuated with 30  $\mu\text{m}$  dia. apertures, undesirable NME geometries were observed, with high-surface area features found only on the edges of the electrodes (consistent with a previous report of NMEs formed with large apertures<sup>38</sup>). This problem was solved by increasing the thickness of the insulating layer to 8  $\mu\text{m}$ , which allowed for the reproducible generation of structures with the desired “fractal”-like geometries (Fig. 2A). We speculate that this is an aspect ratio-effect—the longer diffusion layer (through the thicker insulator) from bulk solution to the surface is linear (as opposed to radial)<sup>39,40</sup> and allows for equal chances for nucleation sites to form at the centre of the electrode as at the edges. Regardless, 8  $\mu\text{m}$  thick SU-8 with 30  $\mu\text{m}$  dia. apertures allowed for reproducible NME formation, and was used for all of the measurements described here.

As shown in Fig. 2A, the stochastic nature of NME formation results in the generation of structures with differing morphologies which (presumably) introduces a level of variance to their surface areas. In most NME experiments, these differences are canceled out by making relative measurements before and after analyte binding to the surface of the electrode;<sup>11,12,14,41–43</sup> unfortunately, this compensatory procedure is not compatible with the magnetic-particle-based methods developed here (described below). Thus, we evaluated NME growth in an attempt to understand (and perhaps improve) their surface-area reproducibility. In initial tests, NMEs were formed using standard methods in which plating potential is applied for a set duration (chosen arbitrarily to be 300 s). But the final plating current (measured at  $t = 300$  s) was found to vary considerably (from 3–7  $\mu\text{A}$ , as per Fig. S1 in the ESI†). We hypothesized that final plating current correlated to surface area; to test the hypothesis, the surface areas

of a group of NMEs formed with different final plating currents were measured using the oxygen desorption method. As described in the ESI† and as shown in Fig. S2,† the final NME plating current is indeed a strong predictor for NME surface area (with  $R^2 = 0.9655$  for a linear regression of the data). Thus, for all work shown here, a new method was adopted, represented in Fig. 2B, in which NMEs were plated to a final plating current limit (chosen to be  $-5.5 \mu\text{A}$ , equivalent to a surface area of 0.4  $\text{mm}^2$  according to Fig. S2†) rather than to a designated plating time. We propose that this method may be useful for improving reproducibility in NME assays for a wide range of applications in the future.

Finally, NMEs have attracted great attention because of their improved analytical sensitivity relative to comparable planar electrodes. To investigate this effect for the NMEs used here, cyclic voltammetry was used to evaluate the performance of three electrode-systems: NMEs on DMF top plates (fabricated as described above), planar “NME-footprint” electrodes (*i.e.*, standard Au working electrode/30  $\mu\text{m}$  dia. aperture structures on DMF top plates used to form NMEs, but with no NMEs formed), and planar electrodes with diameters chosen such that their surface areas (0.50  $\text{mm}^2$ ) are similar to those calculated for the NMEs (as above). An external Pt CE and an Ag/AgCl RE were used to provide a stable reference potential for the three experiments. Representative cyclic voltammograms for  $\text{K}_3\text{Fe}(\text{CN})_6$  in each of the systems are shown in Fig. 2C. The peak currents for the oxidation process at 0.3 V *vs.* Ag/AgCl were 0.79 nA (footprint), 88.65 nA (planar), and 487.76 nA (NME). Thus, the NME electrodes offer a clear advantage in signal (>600-fold) relative to electrodes that have the same planar footprint, which is largely explained by the increased surface area. Perhaps more interestingly, the NME electrodes also offer a significant advantage (>5-fold) relative to electrodes with much larger footprint and similar surface area. We attribute this effect to differences in mass transport; the NME has a microstructure that protrudes into the solution and has an intricate diffusion profile to match its complex morphology. Regardless, it is clear that NME working electrodes bring significant

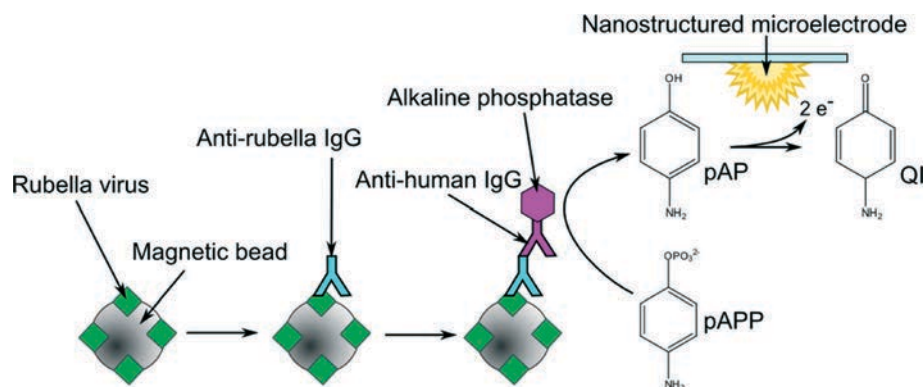


**Fig. 3** Overview of electrochemical bead-based sandwich ELISA for detection of anti-rubella IgG. Virus coated magnetic beads (gray/green) are used to capture anti-rubella IgG (blue) from the sample. Captured IgG is then labeled with anti-human IgG (Fc-specific) conjugated to alkaline phosphatase (pink), which catalyses the hydrolysis of pAPP to pAP. pAP is detected by electrochemical oxidation at the NME, producing quinoneimine (QI).

advantages to sensing, making them attractive for integration with DMF for diagnostics, as described below.

### DMF immunoassays

To evaluate the potential use of DMF-NME devices for diagnostic applications, an assay was developed to screen for rubella virus (RV) immunity, a test that is almost always performed in a centralized laboratory.<sup>44,45</sup> Detection of low concentrations of antibodies in complex samples is challenging, often requiring heterogeneous methods of isolating the analytes combined with numerous repeated washes. DMF has proven useful for these kinds of assays,<sup>20,29–34</sup> typically implemented using magnetic particles, which can be immobilized or moved, depending on the assay-step. Here, we modified a DMF-enabled chemiluminescent assay for RV IgG<sup>35</sup> to generate the electroactive reporter, 4-aminophenol (pAP), as illustrated in Fig. 3. A complex series of wash and immobilization steps was developed to implement the assay, as described below.

Fig. 4 depicts the liquid handling steps involved in the new RV immunoassay. (For clarity, the assay depicted in the figure used coloured droplets on a single sample; in practice, two samples, non-coloured, were processed simultaneously.) Pre-programmed protocols to dispense reagents, remove supernatants, mix magnetic particles, and wash the beads were used to perform all the various steps. The entire assay took approximately 30 min to perform, with 5 min for dispensing reagents and washing the particles and a total of 25 min dedicated to mixing and incubating the magnetic particles with sample, secondary antibody, and pAPP. To perform the eight-step protocol on two samples, six pipetting steps were required to load the two samples, magnetic particles, wash buffer, secondary antibody conjugate, and pAPP. In contrast, to perform the same assay off-chip, a minimum of 50 pipetting operations<sup>46</sup> is required, along with many other user interventions including centrifugation steps (for non-magnetic particles) or magnetic isolation (for magnetic particles). The reduction in pipetting steps (>8-fold in the proof-of-principle work reported here) scales with the number of samples evaluated in parallel; thus, we propose that future instruments relying on DMF devices bearing thousands of driving electrodes<sup>47</sup> will be capable of very significant reductions in the amount of manual intervention required for diagnostic assays.

To evaluate the performance of the new DMF-NME immunoassay, a series of rubella virus IgG calibrators ranging from 0–250 IU mL<sup>-1</sup> was prepared and evaluated in triplicate. As shown in Fig. 5A, the data can be fitted by a four parameter logistic equation ( $R^2 = 0.9632$ ), revealing a limit of detection (LOD) of 0.07 IU mL<sup>-1</sup> and a limit of quantitation (LOQ) of 3.19 IU mL<sup>-1</sup>, both well below the WHO defined cut-off for RV immunity of 10 IU mL<sup>-1</sup>. This performance is directly comparable with a previous DMF-chemiluminescent RV ELISA<sup>35</sup> and to that of traditional, non-electrochemical assays implemented in the laboratory,<sup>44,45</sup> but was implemented

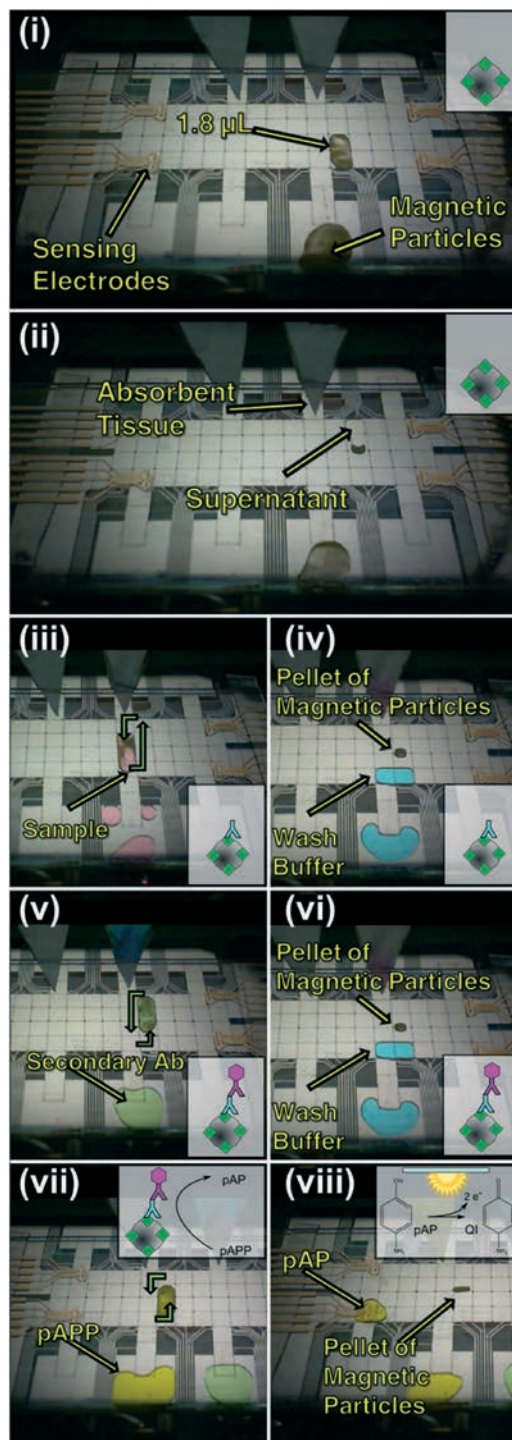
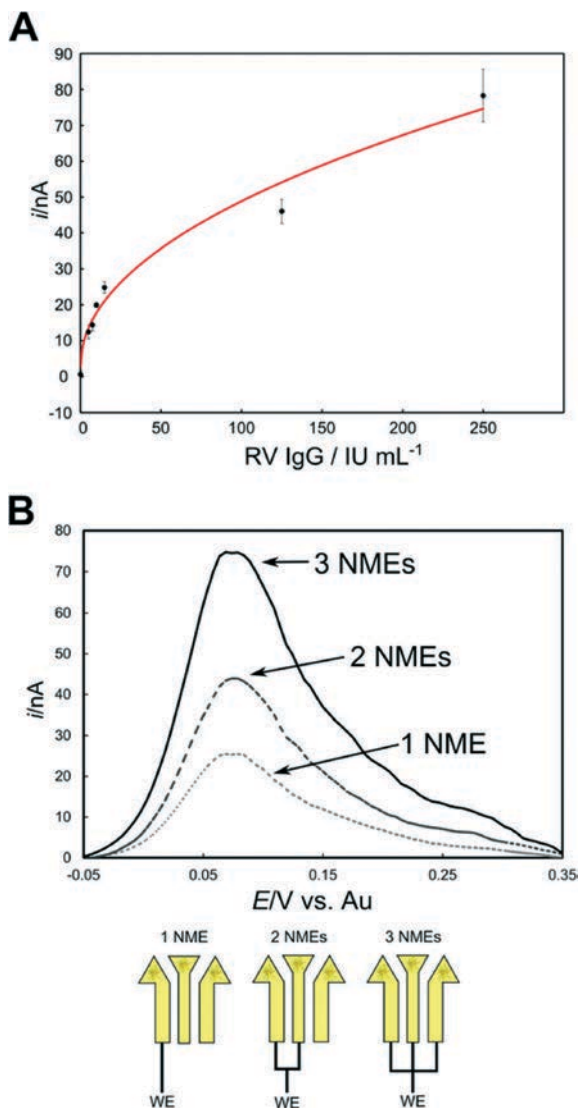


Fig. 4 Screenshots of the DMF immunoassay protocol (dyes added to reagents to enhance droplet visibility). Cartoons in right corner of each panel illustrate the progress of the assay, coded in the colour-scheme from Fig. 3. (i) A droplet of magnetic particles is dispensed and (ii) the magnet is engaged to allow removal of supernatant. (iii) Sample is dispensed and incubated with the particles with active mixing. The supernatant is removed and (iv) the particles are washed four times in buffer. (v) The particles are isolated, then mixed with the secondary antibody and (vi) washed four times. (vii) A solution of pAPP is then dispensed and mixed with the particles for 20 min. (viii) The supernatant (containing pAP) is isolated from the beads and then delivered to the NMEs for electrochemical measurements. Green arrows indicate the droplet movement paths adopted during particle re-suspension steps.



**Fig. 5** DMF-NME ELISA. (A) Calibration curve generated from differential pulse voltammogram measurements of rubella IgG using the automated analysis technique. All conditions were evaluated in triplicate, and error bars are  $\pm 1$  s.d. (B) Differential pulse voltammograms (top) and cartoon schematics (bottom) from an immunoassay on a  $10\ IU\ mL^{-1}$  anti-rubella IgG sample showing additive effects of using 1, 2, or 3 NMEs simultaneously as the working electrode (WE) to measure a single droplet of sample.

here on an integrated, shoebox-sized instrument ( $7 \times 9 \times 12$  inches) that will likely be amenable to deployment for distributed diagnostics in the future. Further, the data in Fig. 5A were generated using individual NMEs as detectors. As illustrated in Fig. 5B, if additional sensitivity is needed (e.g., in cases in which samples must be substantially diluted prior to analysis to limit the effects of cross-reactivity<sup>35</sup>), multiple NMEs can be used in parallel to generate higher signals. Alternatively, in the future, multiple NMEs might be modified with different surface probes to allow for multiplexed sensing.

The method reported here is unique relative to what has been reported previously. The closest analogue that we are

aware of in terms of detection is the NME immunosensor reported by Bhimji *et al.*<sup>15</sup> The new method offers several advantages, including automated sample handling (automated *vs.* manual<sup>15</sup>) and significant reductions in reagent use ( $1.8\ \mu L$  each of sample, labelled conjugate, and substrate *vs.* 20, 20 and,  $50\ \mu L$  respectively<sup>15</sup>). The closest analogue that we are aware of in terms of integrating sample handling with electroanalysis is the DMF immunoassay described by Shamsi *et al.*<sup>20</sup> The assays in the two studies (rubella virus *vs.* thyroid stimulating hormone<sup>20</sup>) are not directly comparable, but the data in Fig. 2C suggests that the new system should be far more sensitive than the system described previously,<sup>20</sup> which employed conventional planar working electrodes. Thus, we propose that the methods described here represent a significant advance for the state of the art in sensitive, integrated clinical assays.

## Conclusions

We report the first integration of nanostructured microelectrodes with a digital microfluidic liquid-handling platform and its application to an electrochemical assay for rubella virus immunity. NMEs were integrated within the top plate of a two-plate DMF device and were shown to have improved sensitivity over planar electrodes. We propose that the enhanced sensitivity afforded by NMEs will be useful in the future for generating quantitative lab-quality results for diagnostic assays performed outside of a centralized laboratory.

## Acknowledgements

We thank the Canadian Institutes for Health Research (CIHR), the National Science and Engineering Research Council (NSERC), and Abbott Diagnostics for support. We thank Drs. Mohtashim Shamsi and Alphonsus Ng (Univ. Toronto) for advice. D. G. R acknowledges support from the Ontario Graduate Scholarship. A. R. W. thanks the Canada Research Chair (CRC) Program for a CRC.

## References

- 1 M. U. Ahmed, I. Saaem, P. C. Wu and A. S. Brown, *Crit. Rev. Biotechnol.*, 2014, **34**, 180–196.
- 2 C. D. Chin, V. Linder and S. K. Sia, *Lab Chip*, 2012, **12**, 2118–2134.
- 3 D. G. Rackus, M. H. Shamsi and A. R. Wheeler, *Chem. Soc. Rev.*, 2015, **44**, 5320–5340.
- 4 J. D. Newman and A. P. F. Turner, *Biosens. Bioelectron.*, 2005, **20**, 2435–2453.
- 5 J. Wang, *Chem. Rev.*, 2008, **108**, 814–825.
- 6 A. P. F. Turner, *Chem. Soc. Rev.*, 2013, **42**, 3184–3196.
- 7 J.-I. Hahn and C. M. Lieber, *Nano Lett.*, 2003, **4**, 51–54.
- 8 G. Herzog and D. W. M. Arrigan, *Analyst*, 2007, **132**, 615–632.
- 9 F. Ricci, G. Adornetto, D. Moscone, K. W. Plaxco and G. Palleschi, *Chem. Commun.*, 2010, **46**, 1742–1744.

- 10 C. Rivet, H. Lee, A. Hirsch, S. Hamilton and H. Lu, *Chem. Eng. Sci.*, 2011, **66**, 1490–1507.
- 11 J. Das, K. B. Cederquist, A. A. Zaragoza, P. E. Lee, E. H. Sargent and S. O. Kelley, *Nat. Chem.*, 2012, **4**, 642–648.
- 12 Y.-G. Zhou, Y. Wan, A. T. Sage, M. Poudineh and S. O. Kelley, *Langmuir*, 2014, **30**, 14322–14328.
- 13 L. Soleymani, Z. Fang, E. H. Sargent and S. O. Kelley, *Nat. Nanotechnol.*, 2009, **4**, 844–848.
- 14 L. Soleymani, Z. Fang, X. Sun, H. Yang, B. J. Taft, E. H. Sargent and S. O. Kelley, *Angew. Chem., Int. Ed.*, 2009, **48**, 8457–8460.
- 15 A. Bhimji, A. A. Zaragoza, L. S. Live and S. O. Kelley, *Anal. Chem.*, 2013, **85**, 6813–6819.
- 16 K. Choi, A. H. C. Ng, R. Fobel and A. R. Wheeler, *Annu. Rev. Anal. Chem.*, 2012, **5**, 413–440.
- 17 V. Srinivasan, V. K. Pamula and R. B. Fair, *Anal. Chim. Acta*, 2004, **507**, 145–150.
- 18 M. D. M. Dryden, D. D. G. Rackus, M. H. Shamsi and A. R. Wheeler, *Anal. Chem.*, 2013, **85**, 8809–8816.
- 19 A. E. Kirby and A. R. Wheeler, *Lab Chip*, 2013, **13**, 2533–2540.
- 20 M. H. Shamsi, K. Choi, A. H. C. Ng and A. R. Wheeler, *Lab Chip*, 2014, **14**, 547–554.
- 21 A. E. Kirby, N. M. Lafrenière, B. Seale, P. I. Hendricks, R. G. Cooks and A. R. Wheeler, *Anal. Chem.*, 2014, **86**, 6121–6129.
- 22 I. Barbulovic-Nad, S. H. Au and A. R. Wheeler, *Lab Chip*, 2010, **10**, 1536–1542.
- 23 S. C. C. Shih, I. Barbulovic-Nad, X. Yang, R. Fobel and A. R. Wheeler, *Biosens. Bioelectron.*, 2013, **42**, 314–320.
- 24 I. A. Eydelnant, B. Betty Li and A. R. Wheeler, *Nat. Commun.*, 2014, **5**, 3355.
- 25 M. J. Jebrail, A. H. C. Ng, V. Rai, R. Hili, A. K. Yudin and A. R. Wheeler, *Angew. Chem., Int. Ed.*, 2010, **49**, 8625–8629.
- 26 M. Jebrail, N. Assem, J. Mudrik, M. Dryden, K. Lin, A. Yudin and A. Wheeler, *J. Flow Chem.*, 2012, **2**, 103–107.
- 27 S. P. Chen, M. R. Javed, H. K. Kim, J. Lei, M. Lazari, G. J. Shah, R. M. van Dam, P. Y. Keng and C. J. Kim, *Lab Chip*, 2014, **14**, 902–910.
- 28 K. Choi, J.-Y. Kim, J.-H. Ahn, J.-M. Choi, M. Im and Y.-K. Choi, *Lab Chip*, 2012, **12**, 1533–1539.
- 29 T. Kokalj, E. Pérez-Ruiz and J. Lammertyn, *New Biotechnol.*, 2015, **32**, 485–503.
- 30 N. Vergauwe, D. Witters, F. Ceyskens, S. Vermeir, B. Verbruggen, R. Puers and J. Lammertyn, *J. Micromech. Microeng.*, 2011, **21**, 054026.
- 31 M.-N. Tsaloglou, A. Jacobs and H. Morgan, *Anal. Bioanal. Chem.*, 2014, **406**, 5967–5976.
- 32 R. S. Sista, A. E. Eckhardt, V. Srinivasan, M. G. Pollack, S. Palanki and V. K. Pamula, *Lab Chip*, 2008, **8**, 2188–2196.
- 33 A. H. C. Ng, K. Choi, R. P. Luoma, J. M. Robinson and A. R. Wheeler, *Anal. Chem.*, 2012, **84**, 8805–8812.
- 34 K. Choi, A. H. C. Ng, R. Fobel, D. A. Chang-Yen, L. E. Yarnell, E. L. Pearson, C. M. Oleksak, A. T. Fischer, R. P. Luoma, J. M. Robinson, J. Audet and A. R. Wheeler, *Anal. Chem.*, 2013, **85**, 9638–9646.
- 35 A. H. C. Ng, M. Lee, K. Choi, A. T. Fischer, J. M. Robinson and A. R. Wheeler, *Clin. Chem.*, 2015, **61**, 420–429.
- 36 Y. H. Yu, J. F. Chen, J. Li, S. Yang, S. K. Fan and J. Zhou, *J. Micromech. Microeng.*, 2013, **23**, 095025.
- 37 Y. H. Yu, J. F. Chen and J. Zhou, *J. Micromech. Microeng.*, 2014, **24**, 015020.
- 38 B. Lam, R. D. Holmes, J. Das, M. Poudineh, A. Sage, E. H. Sargent and S. O. Kelley, *Lab Chip*, 2013, **13**, 2569–2575.
- 39 J. Guo and E. Lindner, *J. Electroanal. Chem.*, 2009, **629**, 180–184.
- 40 A. J. Bard and L. R. Faulkner, *Electrochemical methods: fundamentals and applications*, John Wiley, New York; Chichester, 2001.
- 41 J. Das and S. O. Kelley, *Anal. Chem.*, 2013, **85**, 7333–7338.
- 42 B. Lam, Z. Fang, E. H. Sargent and S. O. Kelley, *Anal. Chem.*, 2011, **84**, 21–25.
- 43 A. T. Sage, J. D. Besant, B. Lam, E. H. Sargent and S. O. Kelley, *Acc. Chem. Res.*, 2014, **47**, 2417–2425.
- 44 M. Enders, U. Bartelt, F. Knotek, K. Bunn, S. Strobel, K. Dietz and G. Enders, *Clin. Vaccine Immunol.*, 2013, **20**, 420–426.
- 45 G. A. Tipples, *J. Infect. Dis.*, 2011, **204**, S659–S663.
- 46 Manual Pipetting Protocol. 1) Dispense particles; 2) Remove supernatant; 3) Dispense sample and mix ; 4) Remove supernatant; 5) Dispense wash buffer and mix; 6) Remove supernatant; 7) Dispense wash buffer and mix; 8) Remove supernatant; 9) Dispense wash buffer and mix; 10) Remove supernatant; 11) Dispense wash buffer and mix; 12) Remove supernatant; 13) Dispense secondary antibody conjugate and mix; 14) Remove supernatant; 15) Dispense wash buffer and mix; 16) Remove supernatant; 17) Dispense wash buffer and mix; 18) Remove supernatant; 19) Dispense wash buffer and mix; 20) Remove supernatant; 21) Dispense wash buffer and mix; 22) Remove supernatant; 23) Dispense substrate to beads and mix; 24) Remove supernatant; 25) Dispense onto electroanalytical cell; ×2 samples.
- 47 B. Hadwen, G. R. Broder, D. Morganti, A. Jacobs, C. Brown, J. R. Hector, Y. Kubota and H. Morgan, *Lab Chip*, 2012, **12**, 3305–3313.